A UV–Induced Genetic Network Links the RSC Complex to Nucleotide Excision Repair and Displays Dose-Dependent Rewiring

Rohith Srivas, Thomas Costelloe, Anne-Ruxandra Carvunis, Sovan Sarkar, Erik Malta, Su Ming Sun, Marijke Pool, Katherine Licon, Tibor van Welsem, Fred van Leeuwen, Peter J. McHugh, Haico van Attikum, Trey Ideker

Supplemental Figures

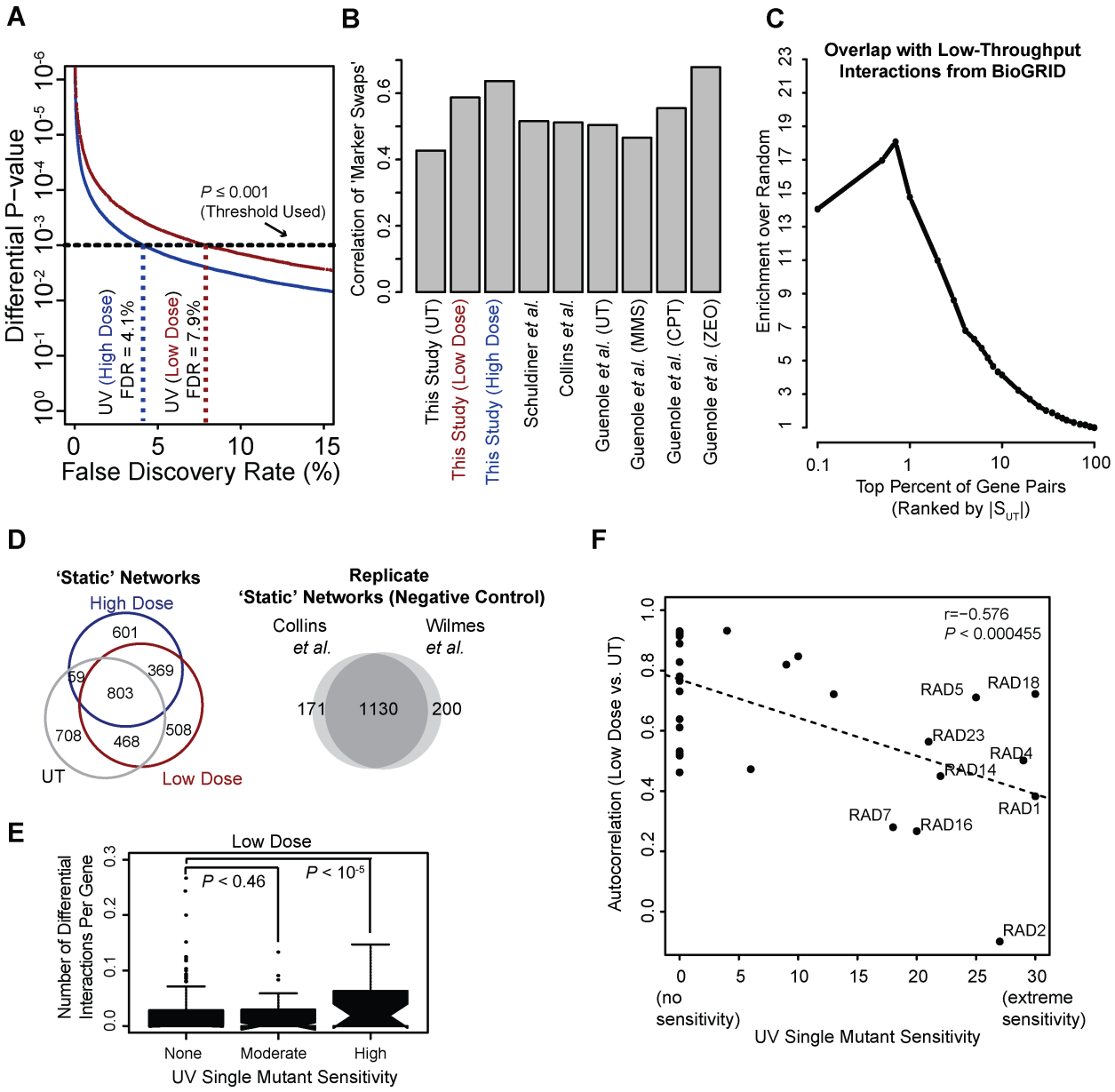

Supplemental Figure S1. Assessing the quality of the UV differential genetic data, Related to Figure 1. (A) The corresponding false discovery rate (assessed using the Benjamini-Hochberg procedure (Benjamini and Hochberg, 1995)) across a range of p-values for the differential networks. (B) Correlation of replicate genetic interaction scores (as measured by the Pearson's correlation coefficient) from 'marker swap' measurements for all static genetic networks in this study. For comparison, the correlation of replicate scores is shown for three previously published data sets (Collins et al., 2007; Guenole et al., 2012; Schuldiner et al., 2005). 'Marker swap' experiments represent replicate measurements obtained for the same double mutant arising from

the two possible pairings of antibiotic resistance markers with gene mutations i.e., *XXX*Δ*::KAN YYY*Δ*::NAT* versus *XXX*Δ*::NAT YYY*Δ*::KAN*. (C) The overlap in static genetic interactions uncovered in untreated conditions versus a set of genetic interactions derived from 'low-throughput' experiments obtained from the Biogrid Database on May 7, 2012 (Chatr-Aryamontri et al., 2013). Enrichment over random is defined as n/r, where n is the number of top-ranked gene pairs (x-axis; ranked by $|S_{UT}|$) found in Biogrid, while r is the number expected at random. (D) Overlap of significant static interactions ($S \geq 2.0$, $S \leq -2.5$) between treated (low and high UV dose) and untreated conditions. As a negative control, the overlap seen amongst two independent genetic interaction screens performed in untreated conditions (Collins et al., 2007; Wilmes et al., 2008) is also shown. (E) Each gene considered in this study is binned according to its UV-induced single mutant sensitivity (Begley et al., 2004) and the distribution of the number of low dose differential interactions per gene (# of significant differential interactions/# of tested differential interactions) in each bin is summarized as a box-and-whisker plot. Significance is assessed using a Mann-Whitney U test. (F) For each query gene, the Pearson's correlation between its low dose static interaction profile and static untreated profile ('Autocorrelation') is plotted against the gene's UV-induced single mutant sensitivity (Begley et al., 2004).

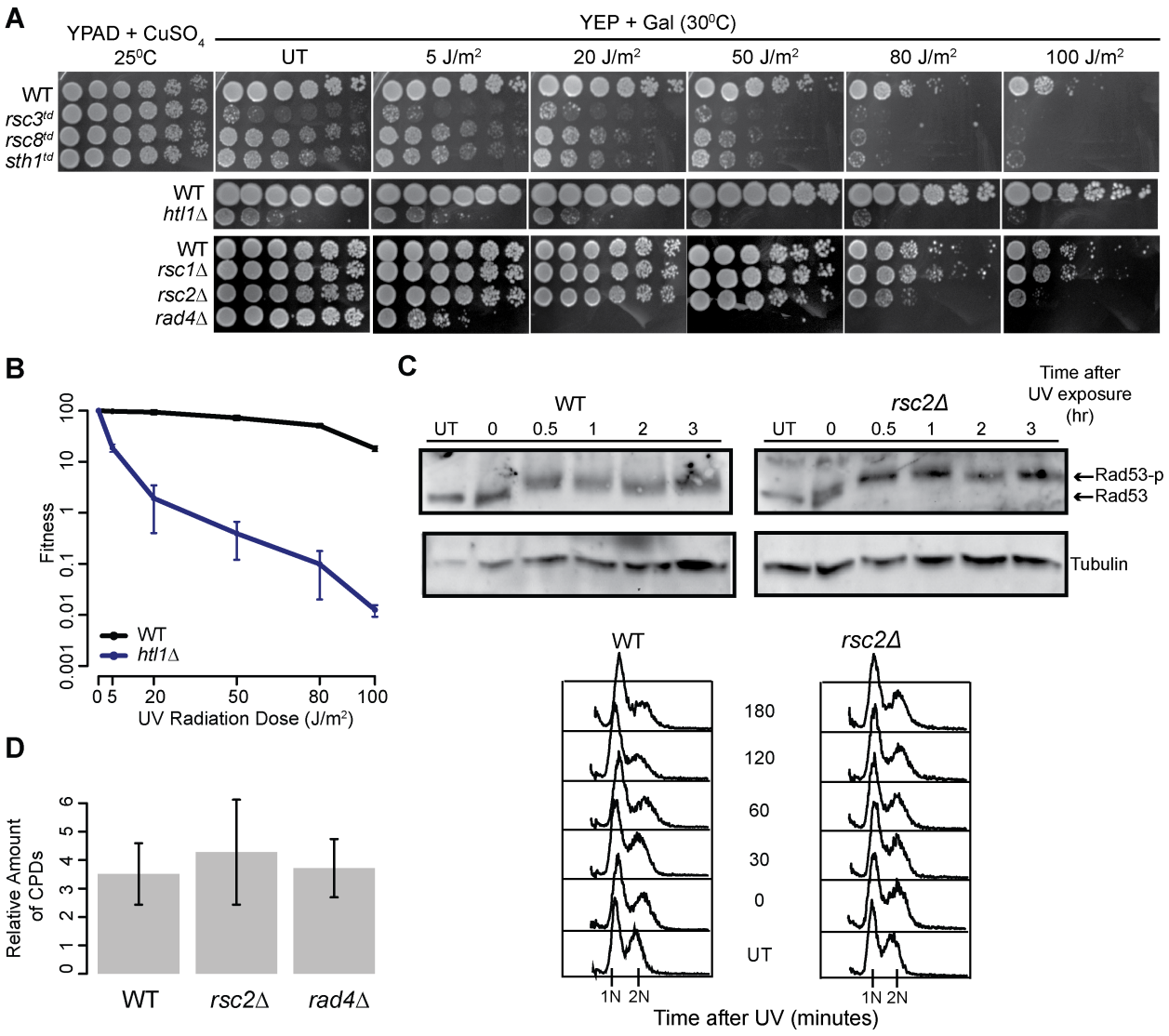

Supplemental Figure S2. RSC mutants are sensitive to UV and its role in facilitating efficient repair appears to be independent of checkpoint regulation, Related to Figure 2. (A) Strains carrying temperature-sensitive degron alleles of essential RSC subunits (*rsc3*^{td}, *rsc8*^{td}, *sth1*^{td}) were grown in either permissive (YPAD + $CuSO_4$, 25°C) or non-permissive conditions (YEP + Gal, 30°C) and exposed to UV- or mock-treatment (UT). Strains carrying deletions of non-essential RSC subunits (*htl1*Δ, *rsc1*Δ, *rsc2*Δ) were spotted onto YPAD plates and then exposed to UV radiation or mock-treatment (UT). All spot dilution assays represent 10-fold serial dilutions of log-phase cells grown for 48 hours. (B) Survival curves for wildtype and *htl1*Δ strains generated through quantification of spot dilution assays in (A) plus one additional replicate (data not shown). Fitness was calculated by counting the number of colonies present in the most dilute spot containing individual colonies and then dividing the count in UV-treated conditions by the count in untreated conditions. All data represent the mean ± 1 s.e.m. of 2 independent replicates. (C) Asynchronously growing mid-log cultures of either wildtype (WT) or *rsc2Δ* cells were exposed to UV radiation (70 J/m^2) and released into fresh YPAD media. Cells

were harvested at the indicated time points to monitor Rad53 phosphorylation by western blot (top) or cell cycle progression by FACS (bottom). (D) Analysis of the amount of cyclobutane pyrmidine dimers (CPDs) present in the genome of WT, *rsc2*Δ, and *rad4*Δ cells immediately after UV irradiation (100 J/m^2). Relative amount of CPDs is defined as the intensity of dot blot bands (probed using anti-CPD antibodies) normalized against the signal obtained from total genomic DNA. Data represent the mean ± 1 s.e.m of three independent replicates.

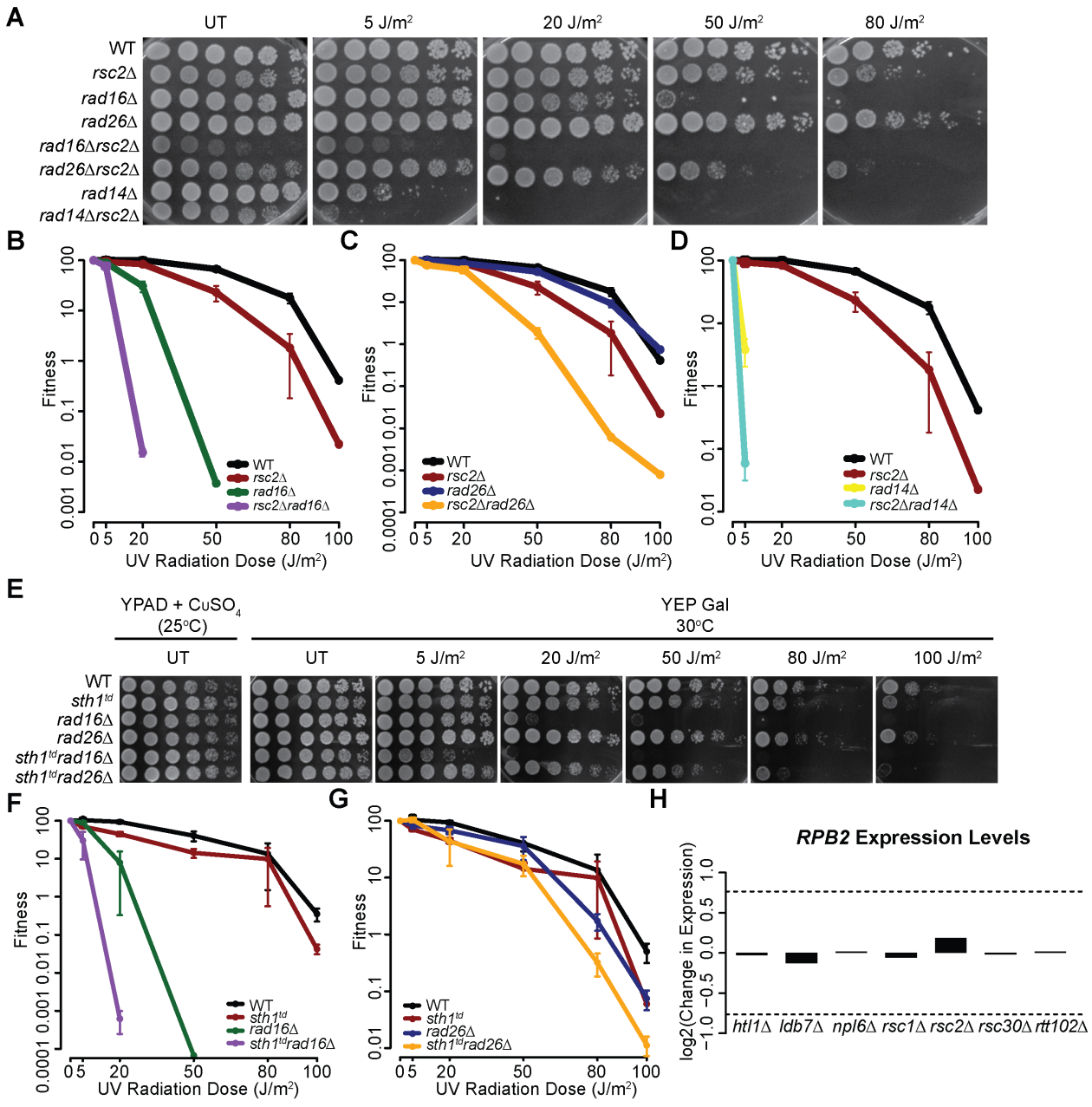

Supplemental Figure S3, Related Figure 2. RSC genetically interacts with components of GGR and TCR. (A,E) 10-fold serial dilutions of log-phase cells carrying single or double deletions of the indicated non-essential genes were spotted on YPAD and exposed to UV radiation or mock-treatment (UT), whereas in (E) strains carrying temperature-sensitive degron alleles of genes encoding subunits of RSC (*sth1*^{td}) were spotted on either permissive (YPAD + $CuSO_4$, 25°C) or non-permissive conditions (YEP + Gal, 30°C) and then exposed to UV- or mock-treatment (UT). All plates were incubated for 48 hours prior to imaging. (B-D, F-G) Survival curves produced by quantifying spot dilution assays in (A,E) plus two additional replicates (data not shown). Quantification was performed as in Figure S2B. All data represent the mean ± 1 s.e.m. of 3 independent replicates. (H) Change in expression of *RPB2* in each of

seven *rsc* mutants compared to wild type cells. Gene expression data were taken from (Lenstra et al., 2011).

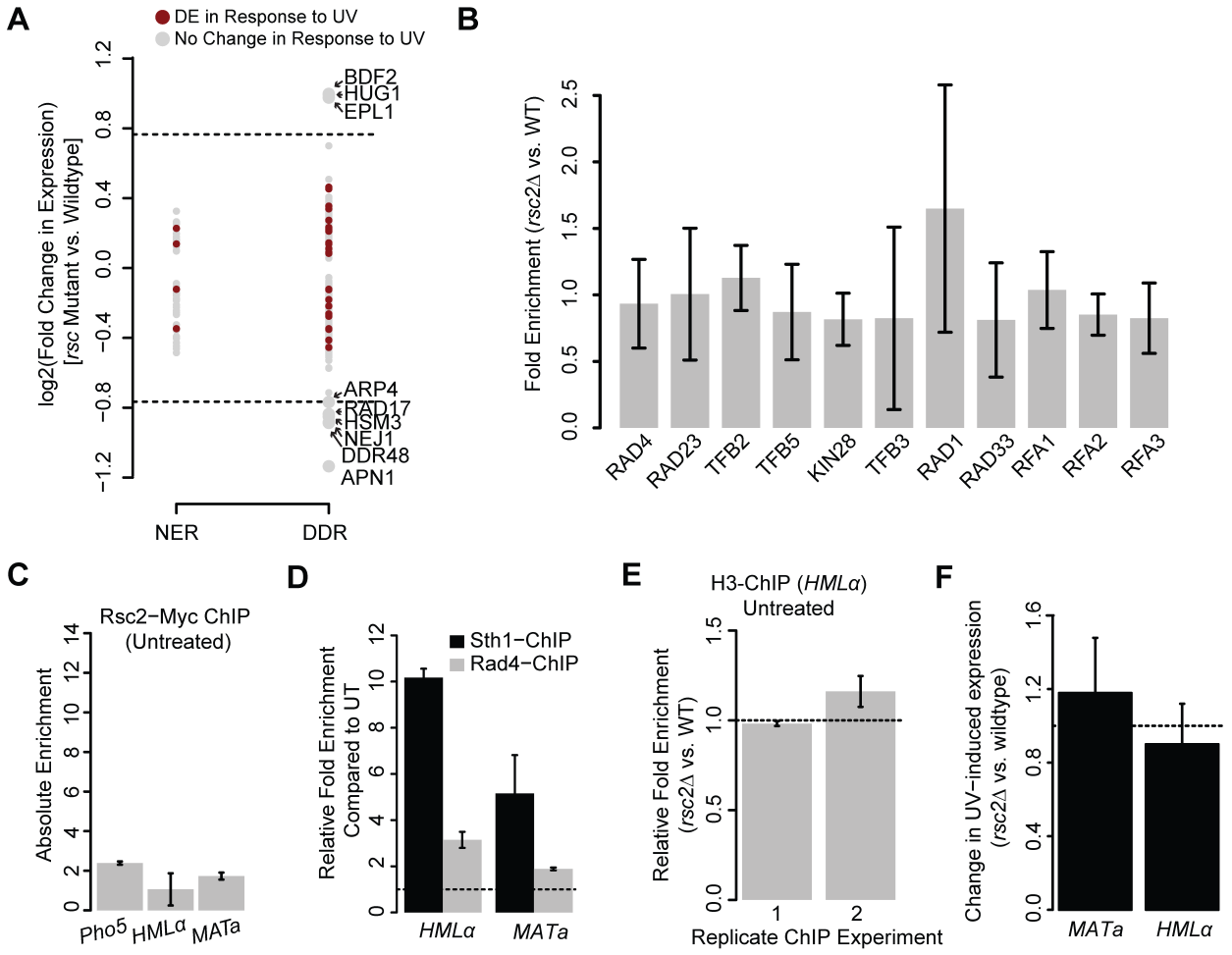

Supplemental Figure S4, Related to Figure 4. RSC's role in facilitating efficient repair appears to be independent of transcriptional regulation. (A) Change in expression of genes involved in NER or the DNA damage response (see Table S7 for a list of process definitions) following deletion of a gene encoding one of the RSC subunits. Each point represents the maximal change in expression seen in any of seven *rsc* mutants (*htl1*Δ, *ldb7*Δ, *npl6*Δ, *rsc1*Δ, *rsc2*Δ, *rsc30*Δ, *rtt102*Δ) compared to wild type cells. Genes which are differentially expressed (DE) following exposure to UV in wild type cells have been colored red. *rsc* mutant gene expression data were taken from (Lenstra et al., 2011); a |fold-change| > 1.7 (dotted line) was used to call a significant change in expression as in the original study. The UV expression data were taken from (Wade et al., 2009). The dataset was downloaded from GEO (GSE16799) and GEO2R was used to download and process the data (default parameters). The final comparison was made between the following samples: 'WT 60 min Rep1/Rep2' and 'WT ND – Rep1/Rep2' and a threshold of P<0.01 was used to call differentially expressed genes. (B) Displays the ratio of the change in expression level of 11 core NER factors following exposure to UV in *rsc2*Δ cells compared to wild type. Data represent the mean ± 1 s.d. of three biological replicates. (C) Absolute enrichment of Rsc2-Myc at the indicated loci in untreated conditions. (D) Analysis of

Sth1-Myc or Rad4-Myc recruitment to either the *MATa* or *HMLα* locus following exposure of G1-synchronized cells to UV radiation. Cells were taken from the experiments described in Figures 4A,B. (E) Relative levels of histone H3 at *HMLα* in *rsc2*Δ versus wildtype in two independent ChIPs. Data in (C,D,E) represent the mean ± 1 s.e.m of two independent replicates. (F) Change in expression level of *MATa* or *HMLα* following exposure to UV in *rsc2*Δ cells compared to wild type. Data represent the mean ± 1 s.e.m. of three independent replicates.

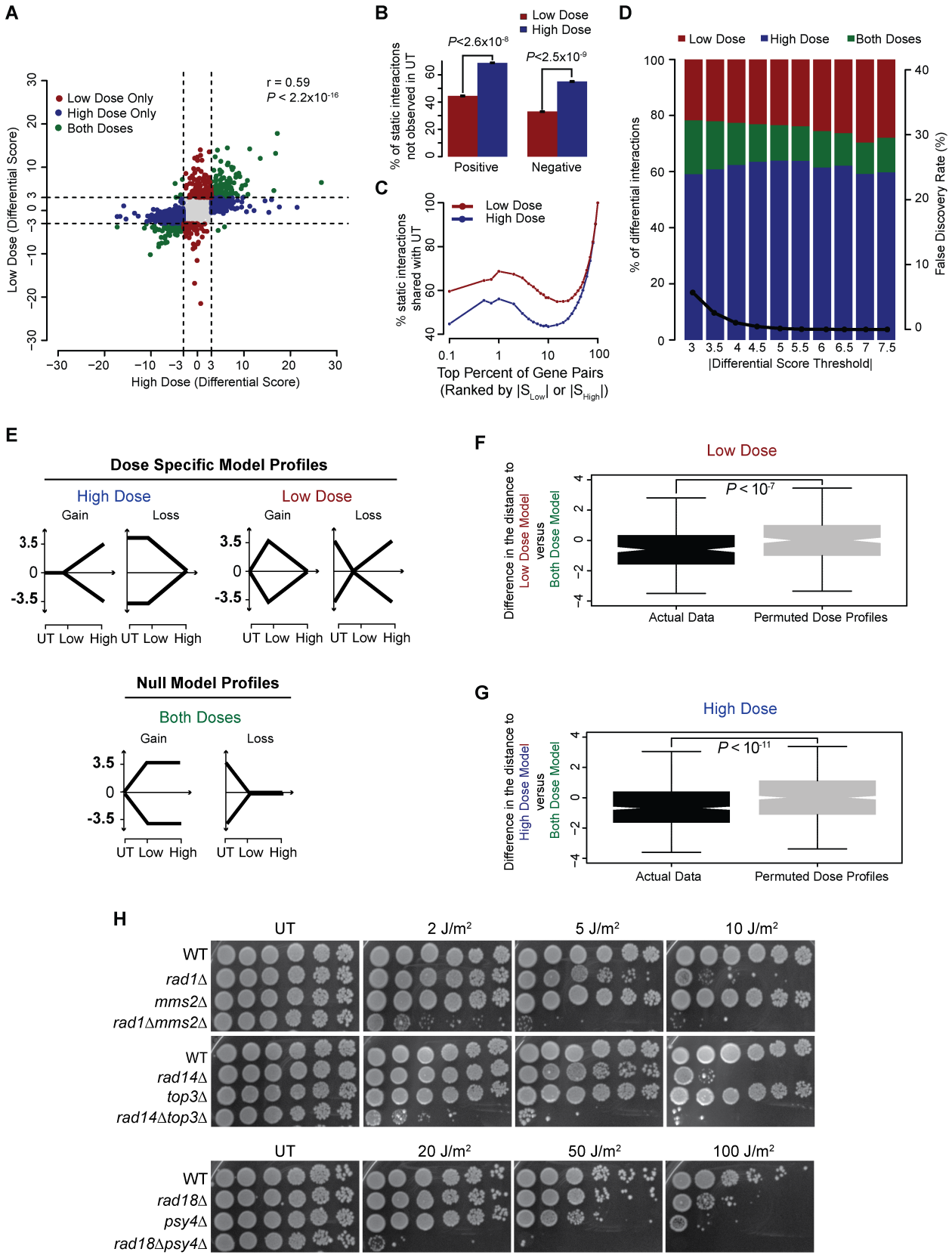
A
Low Dose Only
High Dose Only
Both Doses
r = 0.59
P < 2.2x10-16
Low Dose (Differential Score)
High Dose (Differential Score)
B
Low Dose
High Dose
P<2.6x10-8
P<2.5x10-9
% of static interacitons not observed in UT
Positive
Negative
C
Low Dose
High Dose
% static interactions shared with UT
Top Percent of Gene Pairs
(Ranked by |SLow| or |SHigh|)
D
Low Dose
High Dose
Both Doses
% of differential interactions
False Discovery Rate (%)
|Differential Score Threshold|
E
Dose Specific Model Profiles
High Dose
Low Dose
Gain
Loss
UT Low High
Null Model Profiles
Both Doses
F
Low Dose
P < 10-7
Difference in the distance to
Low Dose Model
versus
Both Dose Model
Actual Data
Permuted Dose Profiles
G
High Dose
P < 10-11
Difference in the distance to
High Dose Model
versus
Both Dose Model
Actual Data
Permuted Dose Profiles
H
UT
2 J/m2
5 J/m2
10 J/m2
WT
rad1Δ
mms2Δ
rad1Δmms2Δ
WT
rad14Δ
top3Δ
rad14Δtop3Δ
UT
20 J/m2
50 J/m2
100 J/m2
WT
rad18Δ
psy4Δ
rad18Δpsy4Δ

Supplemental Figure S5. Comparing low and high dose genetic networks, Related to Figure 5. (A) Scatter of all differential scores between high and low dose genetic maps. Dotted lines represent the threshold used to call a significant differential interaction ($P_{Low-UT,High-UT} \leq 0.001$). (B) Percent of static interactions (positive and negative) in high or low UV dose conditions not observed in the untreated (UT) condition. Error bars were computed using the formula for the standard error of the sample proportion. Significance was assessed using a two-proportion z-test. (C) Fraction of low or high dose static interactions shared with untreated conditions across a range of S score thresholds. (D) Breakdown of the percent of differential interactions specific to either low (red) or high (blue) dose conditions across a range of differential score thresholds. The corresponding false discovery rate at each score threshold is also shown (black line). (E) Dose specific (top) and null model (bottom) static dose profiles used to identify dose-specific differential interactions. See Supplemental Methods for additional details. (F,G) For each (F) low ($P_{Low-UT} \leq 0.001$) or (G) high dose ($P_{High-UT} \leq 0.001$) differential interaction, we computed the Euclidean distance between its static dose profile (S_{UT}, S_{Low}, S_{High}) and the closest (F) low dose or (G) high dose model profile, as well as the closest null model profile. The difference in the distance to the dose specific model versus the distance to the null model profile for all interactions is summarized as a box-and-whisker plot. Permuted dose profiles represent randomized interaction data in which the dose profile for each interaction is permuted 1000 different times. Significance was assessed using a Mann-Whitney U test. (H) 10-fold serial dilutions of log-phase cells of the indicated genotype were spotted onto YPAD plates and exposed to UV radiation or mock-treatment (UT).

Supplementary Tables

Supplemental Table S1. List of all query genes screened in this study, Related to Figure 1.

Supplemental Table S2. List of all array genes screened in this study, Related to Figure 1.

Supplemental Table S3. List of all genetic interactions measured in this study, Related to Figure 1.

Supplemental Table S4. List of multi-gene modules used, Related to Figure 2A.

Supplemental Table S5. List of all module-module interactions identified, Related to Figure 2A.

Supplemental Table S6. List of candidate dose-specific differential interactions, Related to Figure 5. Significant high and low dose specific interactions (FDR<40%) have been highlighted.

Supplemental Table S7. List of process definitions used in analysis, Related to Figures 1A, 1B, 2A, and 2B.

Supplemental Table S8. List of all yeast strains used, Related to Figures 2C, 2D, 3, 4, S2, S3, S4, and S5.

Supplemental Table S9. List of all primer sequences used, Related to Figures 3, 4, and S4.

Supplemental Experimental Procedures

Identifying dose-specific differential genetic interactions

For each high dose or low dose differential interaction, we define its static dose profile ($\vec{S}$):

$$\vec{S} = \langle S_{UT}, S_{Low}, S_{High} \rangle$$

Where S_{UT}, S_{Low}, S_{High} represent, respectively, the static genetic interaction score in untreated, low dose, and high dose conditions. Similarly, we define a set of model high dose specific ($\overrightarrow{\boldsymbol{M_{High}}}$), low dose specific ($\overrightarrow{\boldsymbol{M_{Low}}}$), and both dose ($\overrightarrow{\boldsymbol{M_{High}}}$) static profiles (Figure S5E):

$$\overrightarrow{\boldsymbol{M_{High}}} = \begin{cases} \langle 0,0,3.5 \rangle \\ \langle 0,0,-3.5 \rangle \\ \langle 3.5,3.5,0 \rangle \\ \langle -3.5,-3.5,0 \rangle \end{cases}, \overrightarrow{\boldsymbol{M_{Low}}} = \begin{cases} \langle 0,3.5,0 \rangle \\ \langle 0,-3.5,0 \rangle \\ \langle 3.5,0,3.5 \rangle \\ \langle -3.5,0,-3.5 \rangle \end{cases}, \overrightarrow{\boldsymbol{M_{Both}}} = \begin{cases} \langle 3.5,3.5,0 \rangle \\ \langle 0,0,-3.5 \rangle \\ \langle 3.5,3.5,0 \rangle \\ \langle -3.5,-3.5,0 \rangle \end{cases}$$

A static score of 3.5/-3.5 was chosen to provide a relatively stringent threshold for interaction, corresponding to a FDR < 10% (Collins et al., 2006). Next, for each high dose differential interaction, we compute:

$$MinDist_{High} = \min\left(d\left(\vec{S}, \overrightarrow{\boldsymbol{M_{High}}}\right)\right) - \min\left(d\left(\vec{S}, \overrightarrow{\boldsymbol{M_{Both}}}\right)\right)$$

Where $d(\vec{x}, \vec{y})$ represents the Euclidean distance between points $\vec{x}$ and $\vec{y}$. In essence, we are computing the distance between each interaction and the "closest" dose-specific profile in which an interaction (or lack of interaction) exists in only high dose doses versus the distance to the "closest" both dose profile in which an interaction (or lack of interaction) is observed at both doses. Individual S scores (S_{UT}, S_{Low}, S_{High}) that exceeded 3.5 or -3.5 were capped, respectively, at 3.5 or -3.5. Finally, a high dose specific interaction is indicated when,

$$MinDist_{High} \leq m_0$$

To estimate false discovery rates across a range of thresholds (m_0), we performed the following permutation analysis. Across the entire set of 839 high dose differential interactions ($\boldsymbol{A_{High}}$), we scrambled each interaction's static dose profile ($\vec{S}$), and re-computed $MinDist_{High}$for each randomized interaction. Repeating this procedure 1000 times yielded a null distribution:

$$\boldsymbol{R^0} = \left(\boldsymbol{r_1^0}, \boldsymbol{r_2^0}, \cdots, \boldsymbol{r_{839}^0}\right)$$

Where, $\boldsymbol{r_1^0}$ is the average smallest $MinDist_{High}$ seen across 1000 permutations, $\boldsymbol{r_2^0}$ is the average second-smallest $MinDist_{High}$ seen, etc. We confirmed that the distribution of $MinDist_{High}$ in the actual data was significantly less than in permuted data (Figures S5F,G), after which $\boldsymbol{R^0}$ was used to compute a FDR at a given threshold (m_0) as follows:

$$\text{FDR}(m_0) = \frac{\text{N}(\boldsymbol{R^0} \leq m_0)}{\text{N}(\boldsymbol{A_{High}} \leq m_0)} \times 100$$

Where $\text{N}(\boldsymbol{R^0} \leq m_0)$ and $\text{N}(\boldsymbol{A_{High}} \leq m_0)$ represents, respectively, the number of actual or randomized interactions with a $MinDist_{High}$ less than m_0. The set of 307 low dose interactions were analyzed similarly, except the distance metric was defined as follows:

$$MinDist_{Low} = \min\left(d\left(\vec{S}, \overrightarrow{\boldsymbol{M_{Low}}}\right)\right) - \min\left(d\left(\vec{S}, \overrightarrow{\boldsymbol{M_{Both}}}\right)\right)$$

A list of all 839 high dose and 307 low dose interactions, along with $MinDist_{Low}$or $MinDist_{High}$, and their corresponding FDR is provided in Table S6. At an FDR of 40% we found 35 high dose specific interactions and 44 low dose specific interactions (highlighted interactions in Table S6).

To construct Figure 5A, we first categorized each high dose or low dose differential interaction as a Positive/Negative "Gain of Interaction" or Positive/Negative "Loss of Interaction", as follows:

Let $\text{Sign}(S_{Treated})$ represent the sign of the high or low dose static genetic interaction score, then:

$$\text{Category} = \begin{cases} \text{Positive Gain}, & Sign(S_{Treated}) \rightarrow + \text{ and } |S_{Treated}| > |S_{UT}| \\ \text{Negative Gain}, & Sign(S_{Treated}) \rightarrow - \text{ and } |S_{Treated}| > |S_{UT}| \\ \text{Positive Loss}, & Sign(S_{Treated}) \rightarrow + \text{ and } |S_{Treated}| < |S_{UT}| \\ \text{Negative Loss}, & Sign(S_{Treated}) \rightarrow - \text{ and } |S_{Treated}| < |S_{UT}| \end{cases}$$

Next, interactions within each category were sorted by their $MinDist_{High}$ or $MinDist_{Low}$ value in ascending order and the raw static dose profile was visualized using Java Treeview (v. 1.1.6). As only 65 out of the 307 low dose differential interactions could be classified as "Loss of Interaction", these interactions were not visualized for the sake of clarity.

Novel Connections in the UV differential dataset

Our differential genetic data provides a wealth of data for future studies. To make all the interaction data, as well our analysis accessible to readers, we have packaged it all as a Cytoscape session file available for download on our Supplementary Website (http://chianti.ucsd.edu/~rsrivas/srivas_2013/). Here, we discuss a few examples of interesting connections.

The strongest connection at both doses was between NER and components of the DNA damage response (DDR), including strong differential negative interactions with factors involved in post replication repair (e.g. MMS2; Figure S5H), base excision repair, and double stranded break repair. These negative interactions suggest a certain degree of redundancy among the different DNA repair processes. While NER is the predominant pathway utilized in the repair of UV-induced helix distorting lesions, such lesions can lead to replication fork stalling which can be bypassed by the post replication repair machinery (Auclair et al., 2010), or in the case of fork collapse, counteracted by double-stranded break repair pathways (Chang and Cimprich, 2009; Lundin et al., 2005).

For both UV doses, we observed positive genetic interactions between NER and genes involved in regulating post-translation modifications (PTM) such as ubiquitination (e.g. BRE5) or SUMOylation (e.g. NFI1). Recent work has shown an important role for these PTMs in stabilizing key NER factors such as Rad4 or modulating their affinity for damaged DNA (Bergink et al., 2007; Moschos and Mo, 2006). In this respect, our differential genetic data constitute a resource for identifying possible targets of ubiquitination or SUMOylation amongst NER factors. Past work has shown that components of linear pathways, such as signaling cascades, are often strongly enriched for positive interactions (Fiedler et al., 2009; Guenole et al., 2012; Sharifpoor et al., 2012). Our current dataset contains >50 differential positive interactions connecting NER factors to components of various PTM machinery, providing a wealth of putative targets to follow up on.

Supplemental References

Auclair, Y., Rouget, R., Belisle, J.M., Costantino, S., and Drobetsky, E.A. (2010). Requirement for functional DNA polymerase eta in genome-wide repair of UV-induced DNA damage during S phase. DNA repair *9*, 754-764.

Begley, T.J., Rosenbach, A.S., Ideker, T., and Samson, L.D. (2004). Hot spots for modulating toxicity identified by genomic phenotyping and localization mapping. Molecular cell *16*, 117-125.

Benjamini, Y., and Hochberg, Y. (1995). Controlling the false discovery rate: a practical and powerful approach to multiple testing. Journal of the Royal Statistical Society Series B (Methodological), 289-300.

Bergink, S., Jaspers, N.G., and Vermeulen, W. (2007). Regulation of UV-induced DNA damage response by ubiquitylation. DNA repair *6*, 1231-1242.

Chang, D.J., and Cimprich, K.A. (2009). DNA damage tolerance: when it's OK to make mistakes. Nature chemical biology *5*, 82-90.

Chatr-Aryamontri, A., Breitkreutz, B.J., Heinicke, S., Boucher, L., Winter, A., Stark, C., Nixon, J., Ramage, L., Kolas, N., O'Donnell, L.*, et al.* (2013). The BioGRID interaction database: 2013 update. Nucleic acids research *41*, D816-823.

Collins, S.R., Miller, K.M., Maas, N.L., Roguev, A., Fillingham, J., Chu, C.S., Schuldiner, M., Gebbia, M., Recht, J., Shales, M.*, et al.* (2007). Functional dissection of protein complexes involved in yeast chromosome biology using a genetic interaction map. Nature *446*, 806-810.

Collins, S.R., Schuldiner, M., Krogan, N.J., and Weissman, J.S. (2006). A strategy for extracting and analyzing large-scale quantitative epistatic interaction data. Genome biology *7*, R63.

Fiedler, D., Braberg, H., Mehta, M., Chechik, G., Cagney, G., Mukherjee, P., Silva, A.C., Shales, M., Collins, S.R., van Wageningen, S.*, et al.* (2009). Functional organization of the S. cerevisiae phosphorylation network. Cell *136*, 952-963.

Guenole, A., Srivas, R., Vreeken, K., Wang, Z.Z., Wang, S., Krogan, N.J., Ideker, T., and van Attikum, H. (2012). Dissection of DNA Damage Responses Using Multiconditional Genetic Interaction Maps. Molecular cell.

Lenstra, T.L., Benschop, J.J., Kim, T., Schulze, J.M., Brabers, N.A., Margaritis, T., van de Pasch, L.A., van Heesch, S.A., Brok, M.O., Groot Koerkamp, M.J.*, et al.* (2011). The specificity and topology of chromatin interaction pathways in yeast. Molecular cell *42*, 536-549.

Lundin, C., North, M., Erixon, K., Walters, K., Jenssen, D., Goldman, A.S., and Helleday, T. (2005). Methyl methanesulfonate (MMS) produces heat-labile DNA damage but no detectable in vivo DNA double-strand breaks. Nucleic acids research *33*, 3799-3811.

Moschos, S.J., and Mo, Y.Y. (2006). Role of SUMO/Ubc9 in DNA damage repair and tumorigenesis. Journal of molecular histology *37*, 309-319.

Schuldiner, M., Collins, S.R., Thompson, N.J., Denic, V., Bhamidipati, A., Punna, T., Ihmels, J., Andrews, B., Boone, C., Greenblatt, J.F.*, et al.* (2005). Exploration of the function and organization of the yeast early secretory pathway through an epistatic miniarray profile. Cell *123*, 507-519.

Sharifpoor, S., van Dyk, D., Costanzo, M., Baryshnikova, A., Friesen, H., Douglas, A.C., Youn, J.Y., VanderSluis, B., Myers, C.L., Papp, B.*, et al.* (2012). Functional wiring of the yeast kinome revealed by global analysis of genetic network motifs. Genome research *22*, 791-801.

Wade, S.L., Poorey, K., Bekiranov, S., and Auble, D.T. (2009). The Snf1 kinase and proteasome-associated Rad23 regulate UV-responsive gene expression. The EMBO journal *28*, 2919-2931.

Wilmes, G.M., Bergkessel, M., Bandyopadhyay, S., Shales, M., Braberg, H., Cagney, G., Collins, S.R., Whitworth, G.B., Kress, T.L., Weissman, J.S.*, et al.* (2008). A genetic interaction map of RNA-processing factors reveals links between Sem1/Dss1-containing complexes and mRNA export and splicing. Molecular cell *32*, 735-746.